Int. J. Environ. Sci. Technol. (2016) 13:65–76
DOI 10.1007/s13762-015-0841-y

ORIGINAL PAPER

# Adsorption of Pb(II) and Cu(II) metal ions on functionalized large-pore mesoporous silica

J.-Y. Lee[1,2] · C.-H. Chen[2] · S. Cheng[2] · H.-Y. Li[1]

Received: 18 January 2015 / Revised: 22 April 2015 / Accepted: 30 June 2015 / Published online: 4 August 2015


**Abstract** Adsorption of copper and lead ions in aqueous solutions onto large-pore mesoporous silica materials functionalized with amino and mercapto groups and those with different morphologies including fiber-like, rod-like, and platelet was studied. The synthesized materials were characterized by techniques such as X-ray powder diffraction, nitrogen adsorption–desorption isotherms, scanning electron microscopy, and infrared spectra. Batch experiments were conducted to determine the adsorption processes. The equilibrium adsorption data agreed with Langmuir isotherms and revealed that four amino groups were required to form a stable surface complex with copper ions. Results indicated that initial adsorption rate onto platelet mesoporous adsorbent was rapid and faster than that of rod-like and fibrous morphologies due to its short channeling pores. Thiol-functionalized mesoporous silica adsorbents of all the morphologies have a better affinity for $Pb^{2+}$ than the amino-mesoporous silica. In contrast, amino-mesoporous silica has a stronger affinity for $Cu^{2+}$ compared to thiol-mesoporous silica. The optimal $Pb^{2+}$ uptake on thiol-mesoporous silica was in solution with pH in 2–6, while the highest $Cu^{2+}$ uptake on amino-mesoporous silica was at pH 5.

**Keywords** Adsorbent · Functionalized silica · Heavy metals · Kinetics · Morphology · Surface complex

## Introduction

Many industries such as textiles, mining, painting, electroplating, plumbing, fertilizer, and battery manufacturing generate wastewater with various heavy metals such as Pb(II) and Cu(II). If the wastewater is discharged into the environment without treatment, it would cause serious biohazards and threaten the health of human beings. Owing to the toxicity of these metals, the World Health Organization (2006) restricts the maximum acceptable concentrations of Pb and Cu ions in drinking water to be 0.01 and 2.0 mg/L, respectively.

Therefore, the removal of these heavy metals from industrial wastewater has attracted great attentions of scientists. Several methods have been developed to remove heavy metal ions from aqueous solutions, and adsorption is one of the most frequently used techniques. The adsorbents adopted in the literature include waste dust (Wang and Lin 2008; Amarasinghe and Williams 2007; Sharaf and Hassan 2014; Singh et al. 2014), clays (Özcan et al. 2009), polymer fibers (Deng et al. 2003), and porous silica (Feng et al. 1997; Liu et al. 2000; Lam et al. 2006; Walcarius et al. 2003; Vasudevan et al. 2011; Blitz et al. 2007; Aguado et al. 2009, 2008; Xia et al. 2010; Da'na and Sayari 2011; Shahbazi et al. 2011; Liang et al. 2009; Kao et al. 2008; Chandra et al. 2010). Still, researches toward the development of efficient adsorbents for the removal of heavy metals from wastewater are of great concern.

**Electronic supplementary material** The online version of this article (doi:10.1007/s13762-015-0841-y) contains supplementary material, which is available to authorized users.

✉ J.-Y. Lee
jylee@nuu.edu.tw

[1] Department of Chemical Engineering, National United University, Miaoli 36003, Taiwan

[2] Department of Chemistry, National Taiwan University, No. 1, Sec. 4, Roosevelt Road, Taipei 10617, Taiwan

The SBA-15 (the abbreviation of number 15 Santa Barbara Amorphous) material has attracted great attention in comparison with other mesoporous silica such as M41S, due to its relatively large pore diameter and good hydrothermal stability (Beck et al. 1992; Zhao et al. 1998a, b). For faster molecular diffusion and mass transfer inside the pores during the applications in adsorption, the pore length of SBA-15 is also important (Yu et al. 2004, 2002; Zhao et al. 2000). According to the original paper reported by Zhao et al. (1998a, b), SBA-15 materials have fiber-like morphology and channeling pores parallel to the long axis of the fibers in the micrometers length (Zhao et al. 1998a, b). The same research group later synthesized SBA-15 materials with a rod-like morphology and average pore length of ca. 1–2 μm by adding salts such as KCl and NaCl and keeping the synthesis solution in static condition (Yu et al. 2002, 2004; Zhao et al. 2000). Recently, SBA-15 mesoporous silica with very short mesopore channels in the sub-micrometer scale has also been synthesized (Kosuge et al. 2004; Sayari et al. 2004; Chen et al. 2008, 2012; Zhang et al. 2006; Linton and Alfredsson 2008; Sujandi and Park 2008; Wang et al. 2005). These short-channel SBA-15 materials offer significant advantages in the faster rate and the larger capacity for adsorption of bulky molecules, as well as in enzyme immobilization.

One of the important adsorption mechanisms is that metal ions interact with the surfaces of adsorbent through complexation or ion exchange (Chandra et al. 2010; Lacour et al. 2001). According to the literature (Deng et al. 2003), the adsorbents with carboxylate, sulfonic, and phosphoric groups on the surfaces favor metal ion adsorption through the ion exchange mechanism, while those containing amine groups on the surfaces adsorb metal ions through the complexation and chelation mechanisms. Hence, adsorption of metal ions can be controlled by introducing different functional groups onto the surfaces of the adsorbent.

Two methods are commonly adopted to prepare organic functionalized SBA-15 materials: one-pot co-condensation and post-grafting methods. The co-condensation method is often preferred to the post-grafting pathway because it minimizes processing steps and provides more uniform distribution of organic functionalities without blocking the entrance of the mesopores (Chen et al. 2008; Sujandi and Park 2008; Wang et al. 2005; Dufaud and Davis 2003; Melero et al. 2006; Agnado et al. 2008). Functional groups such as amino (Liu et al. 2000; Walcarius et al. 2003; Aguado et al. 2009; Da'na and Sayari 2011; Shahbazi et al. 2011) and thiol (Feng et al. 1997; Walcarius et al. 2003; Agnado et al. 2008) have been incorporated onto the SBA-15 framework. Many works show that the adsorption capacity of mesoporous silica is related to the density of active sites and their textural properties (Lam et al. 2006; Xia et al. 2010; Agnado et al. 2008). So far, the literature considering the influence of morphology of mesoporous organosilica on the adsorption of metal ions is limited on the silica gels (Vasudevan et al. 2011; Blitz et al. 2007; Xia et al. 2010). Well-ordered thiol-functionalized SBA-1 with isotropic or spherical-shaped morphology has been synthesized by Kao et al. (2008) using co-condensation method, but the different morphology materials have not been used in the adsorption of metal ions yet.

In this study, amino- and thiol-functionalized mesoporous SBA-15 with platelet, rod-like, and fibrous-like morphologies were prepared via co-condensation. The physicochemical properties of the synthesized materials were characterized by various techniques. These functionalized SBA-15 materials were used as adsorbents to investigate their behaviors in removing $Cu^{2+}$ and $Pb^{2+}$ from aqueous solutions. The equilibrium data and adsorption kinetics were obtained in a batch process. The factors affecting adsorption including morphologies of adsorbents, pH of solution, substituent groups on SBA-15 framework, and content of functional groups were discussed.

The synthesis and characterization of adsorbents were done at Department of Chemistry, National Taiwan University, Taipei, Taiwan, in a 21-month period between September 2010 and May 2012, and the studies of adsorption kinetics and thermodynamics of the Cu(II) and Pb(II) ions have been performed at Department of Chemical Engineering, National United University, Miaoli, Taiwan, till March 2015.

## Materials and methods

### Materials

All chemicals were used as received. Surfactant Pluronic P123 ($EO_{20}PO_{70}EO_{20}$, $M_{av} = 5800$) was purchased from Aldrich. Tetraethylorthosilicate (TEOS, 98 %), aminopropyltrimethoxysilane (APTMS, 98 %), mercaptopropyltrimethoxysilane (MPTMS, 95 %), $ZrOCl_2{\cdot}8H_2O$, NaCl, hydrochloric acid (37 %), ascorbic acid, ammonium hydroxide, copper(II) nitrate trihydrate, methanol, and ethanol (95 %) were from Acros, and lead(II) nitrate was from Alfa.

### Preparation of adsorbents

*Preparation of $NH_2$-SBA-15 with different morphologies*

Conventional $NH_2$-SBA-15 of rod shape was prepared by dissolving 4.0 g of Pluronic P123 in 160 g of 2.0 M HCl solution at 35 °C. The amount of 8.4 g TEOS was added into the above solution and pre-hydrolyzed for 2 h, and then, 1.0 g of APTMS was added. The gel compositions

were 0.017 P123: 1.0 TEOS: 0.12 APTMS: 7.9 HCl: 204 $H_2O$. The mixture solution sealed in a polypropylene bottle was stirred at 35 °C for 24 h and then hydrothermally treated at 90 °C for another 24 h under a static condition. The solid precipitates collected by filtration were washed with de-ionized water and dried overnight at 50 °C. The P123 was removed by ethanol extraction at 78 °C for 1 day. The resultant material was denoted as $NH_2$-SBA-15-r with a rod-like morphology.

The morphologies of rod-$NH_2$-SBA-15 could be changed to other forms by adding NaCl or $ZrOCl_2{\cdot}8H_2O$ (Chen et al. 2008). The platelet $NH_2$-SBA-15 (denoted as $NH_2$-SBA-15-p) was synthesized by adding 0.66 g of $ZrOCl_2{\cdot}8H_2O$ into the conventional $NH_2$-SBA-15 synthesis solution. The compositions were 0.017 P123: 1.0 TEOS: 0.12 APTMS: 0.05 $ZrOCl_2{\cdot}8H_2O$: 7.9 HCl: 204 $H_2O$. The fiber $NH_2$-SBA-15 (denoted as $NH_2$-SBA-15-f) was synthesized by adding 14 g of NaCl into the conventional $NH_2$-SBA-15 synthesis solution. The compositions were 0.017 P123: 1.0 TEOS: 0.12 APTMS: 6 NaCl: 7.9 HCl: 204 $H_2O$. Before the reaction, the aminopropyl-functionalized materials were treated with tetramethylammonium hydroxide (TMAOH) to remove the residue $Cl^-$ ions and to neutralize the protonated amine groups in the sample. Typically, one gram of the modified sample was suspended in 50 mL of 0.2 M methanol solution of TMAOH at room temperature for 30 min. The solid was recovered by filtration, washed with methanol, and finally dried at 120 °C for 1 day.

*Preparation of SH-SBA-15 with different morphologies*

The thiol-functionalized SBA-15 silica was synthesized by replacing APTMS in the procedure previously stated with MPTMS. The as-made SH-SBA-15 was then extracted with ethanol in the presence of ascorbic acid. The ratio of SH-SBA-15: ethanol: ascorbic acid was 3.6 g: 1.5 L: 5 g. The purpose of adding ascorbic acid in the extraction solution is that it can reduce the possibility of –S–S– bond formation and retain the thiol (–SH) groups on the surface of the adsorbent. Before use, the thiol-SBA-15 was washed again by refluxing with deionized water for 1 h and filtered, washed with methanol, and dried at 50 °C for 30 min.

## Characterization

X-ray powder diffraction (XRD) data were collected on a Panalytical X'Pert Pro diffractometer using Cu Kα radiation (λ = 1.5418 Å) at 45 kV and 40 mA from 0.5° to 5° (2θ).

$N_2$ adsorption–desorption isotherms were carried out using Micromeritics Tristar 3000 at liquid nitrogen temperature. Before the measurement, the samples were degassed at 120 °Cfor 12 h. The specific surface areas were evaluated using Brunauer–Emmett–Teller (BET) method in the $P/P^0$ range of 0.05–0.3. Pore size distribution curves were calculated using the desorption branch of the isotherms and the Barrett–Joyner–Halenda (BJH) method. Elemental analyses (EA) of C and N contents were measured by using a Heraeus VarioEL CHNS analyzer. Fourier transform infrared (FTIR) spectroscopy was carried on a spectrometer with a resolution of 2 $cm^{-1}$, and the KBr method was applied. The scanning electron microscopy was carried out on a Hitachi S-800 electron microscope. The zeta potential of a sample was measured by using a Malvern Zetasizer 3000HS instrument. The sample was dispersed in an aqueous solution with a proper concentration.

## Adsorption experiment

*Batch equilibrium studies*

The adsorption behaviors of organic functionalized mesoporous SBA-15 silica were investigated for removing Cu(II) and Pb(II) ions from the aqueous solutions of their nitrate salts in a batch system at 30 °C. Initial concentrations of $Cu^{2+}$ and $Pb^{2+}$ were prepared to be 20, 30, 40, 50, and 60 ppm ($g/m^3$). Typically, 30 mg of functionalized SBA-15 powders were introduced into a 50-$cm^3$ flask containing 30 $cm^3$ of the aqueous solution containing a single metal ion species. Solution pH was adjusted with diluted $HNO_3$ and NaOH solutions. The flasks were transferred to a shaker bath at 150 r/min for about 3 h to reach equilibrium. The adsorbent was removed by centrifugation, and the equilibrium concentration was determined by atomic absorption spectrophotometer (AA6300 Shimadzu). The adsorption capacity, Q (mmol/g), was determined using the following expression:

$$Q = \frac{(C_o - C_f)V}{m} \quad (1)$$

where $C_0$ and $C_f$ are the initial and final (after adsorption) metal ions concentrations (mmol/L), respectively, $V$ is the volume (L) of metal ions solution, and m is the mass (g) of the adsorbent.

*Batch kinetics studies*

In the experiment of kinetic studies, 30 mg of functionalized SBA-15 powder and 30 $cm^3$ of 60 ppm Cu(II) or Pb(II) ion aqueous solution were poured in a 50-$cm^3$ flask and stirred using a shaker with a water bath to control temperature. After various periods, 1 g of the metal ion solution was taken out and diluted with deionized water to 10 g, and its concentration was determined by atomic absorption spectrophotometer (AA6300 Shimadzu).

## Results and discussion

### Characterization of adsorbents

Figure 1 shows the small-angle XRD patterns and $N_2$ adsorption–desorption isotherms of $NH_2$-SBA-15 and SH-SBA-15 materials with different morphologies. The resultant materials have three distinct diffraction peaks indexed to the (100), (110), and (200) planes of 2D hexagonal *p6mm* symmetry appearing in the region of 2θ from 0.7° to 2°. The $N_2$ adsorption–desorption isotherms and the BJH desorption pore size distribution (Fig S1) of $NH_2$-SBA-15 materials show that all of the samples exhibit characteristic type IV isotherms and have a steep increase in adsorption at $P/P_0 = 0.6$–0.8. It indicates that all of these SBA-15 materials possess large mesoporous channels and narrow pore size distributions. The derived textural properties are summarized in Table 1. Compared with siliceous SBA-15-p, the pore diameters and volumes as well as BET surface areas of functionalized materials are all lower. The pore diameters of $NH_2$-SBA-15-p and SH-SBA-15-p decrease by 28 and 22 %, respectively; the BET surface areas decrease by 34 and 34 %, respectively; and the pore volumes decrease by 32 and 32 %, respectively. In contrast, the wall thicknesses of functionalized materials increase. It implies that the organic functional groups are incorporated on the silica framework and occupy a portion of the pore volume. As a result, the pore diameters shrink. Elemental analysis of functional group (abbreviated as FG) is summarized in Table 1. Based on the results, the contents of functional groups decreased in the order of fiber > platelet > rod, and about 61–85 % of the organic silanes in the synthesis gels were effectively incorporated as functional groups in the silica framework.

The SEM photographs (Fig. 2) show that the fiber-like morphology has long channels whose axes are parallel to the long axis of the fiber, while the platelet morphology has short channels whose axes are aligned along the short side of the platelet. It demonstrates that the channel lengths of functionalized SBA-15 silica vary with the different morphologies, and the channel lengths of the platelet materials are shorter than those of the fiber-like and the rod-like materials (Chen et al. 2008).

Figure 3 illustrates the FTIR spectra of $NH_2$-SBA-15 and SH-SBA-15 with various morphologies. In all the materials, the typical Si–O–Si bands associated with the condensed silica networks are observed around 1220, 1070, 795, and 470 $cm^{-1}$(Wang et al. 2005). For amino-functionalized SBA-15, although $NH_2$ stretching vibration is hidden in the broad band from 2700 to 3400 $cm^{-1}$, the

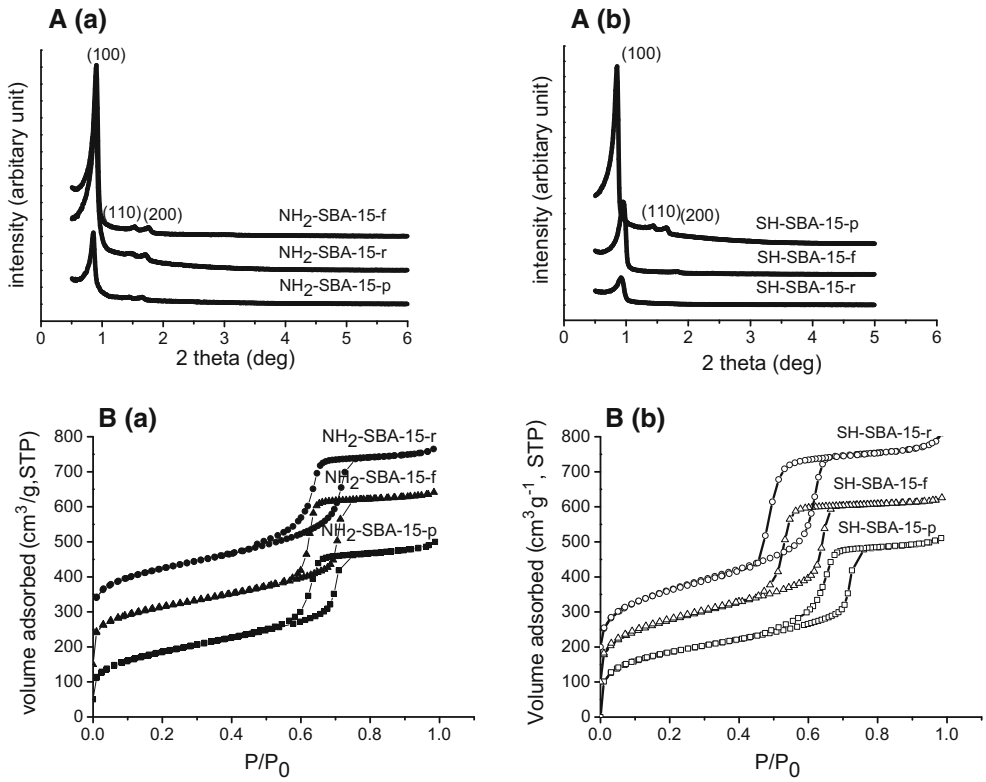


**Fig. 1** **A** Small-angle XRD patterns and **B** $N_2$ adsorption–desorption isotherms (values in *y*-axis shift for 100 units apart) of ***a*** $NH_2$-SBA-15 and ***b*** SH-SBA-15 with different morphologies

**Table 1** Textural and chemical properties of functionalized SBA-15 synthesized with different organic groups

| Material | FG/Si[d] (molar ratio) | $d_{100}$ (nm) | $a_o^a$ (nm) | $\Phi_p^b$ (nm) | $S_{BET}$ ($m^2/g$) | $V_{total}$ ($cm^3/g$) | $w^c$ (nm) |
|---|---|---|---|---|---|---|---|
| SBA-15-p | 0 | 9.70 | 10.5 | 7.2 | 767 | 0.99 | 3.3 |
| $NH_2$-SBA-15-p | 8.7 % (12 %) | 9.71 | 11.2 | 5.2 | 504 | 0.67 | 6.0 |
| $NH_2$-SBA-15-f | 9.3 % (12 %) | 10.3 | 11.9 | 5.2 | 580 | 0.75 | 6.7 |
| $NH_2$-SBA-15-r | 8.2 % (12 %) | 9.93 | 11.5 | 5.5 | 626 | 0.78 | 6.0 |
| SH-SBA-15-p | 9.6 % (12 %) | 10.4 | 12.0 | 5.6 | 504 | 0.67 | 6.4 |
| SH-SBA-15-f | 10.2 % (12 %) | 9.2 | 10.6 | 3.8 | 652 | 0.79 | 6.8 |
| SH-SBA-15-r | 7.3 % (12 %) | 9.5 | 11.0 | 3.4 | 637 | 0.84 | 7.6 |

[a] $a_0 = 2d_{100}/\sqrt{3}$

[b] Pore diameter determined by the maximum of BJH pore size distribution profile based on desorption profile

[c] Wall thickness $w = a_o - \Phi_p$

[d] From elemental analyses, those in parentheses are the ratios in the synthesis solution

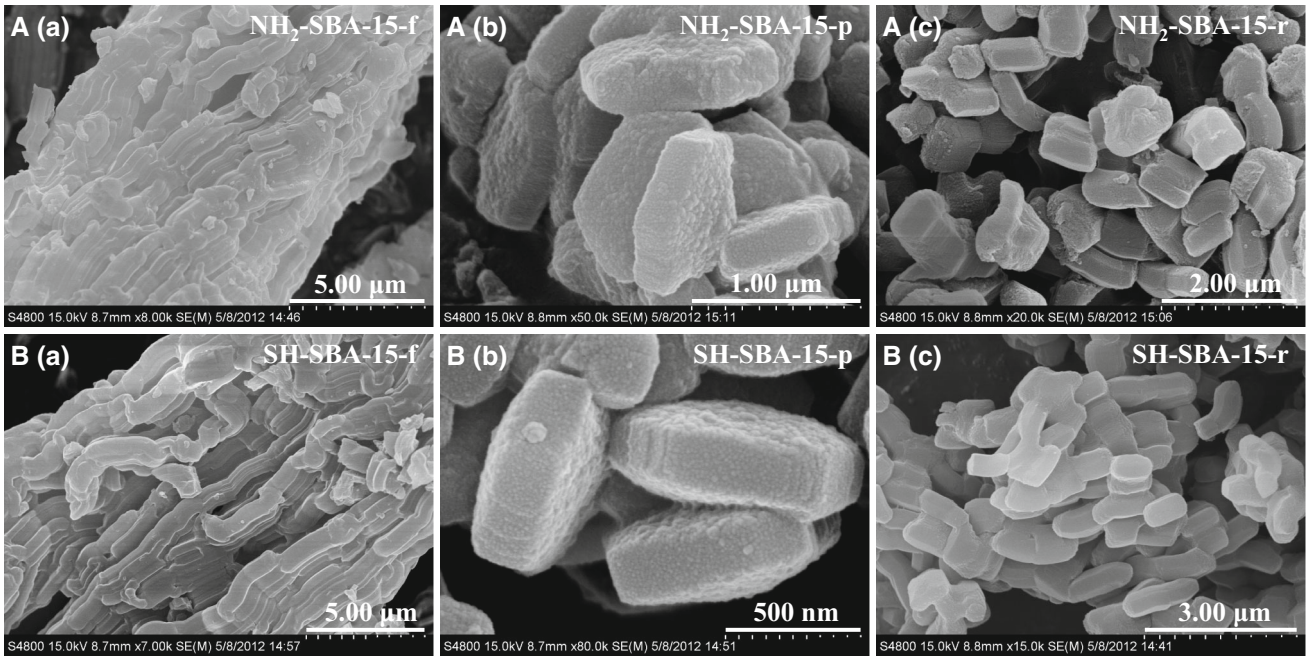


**Fig. 2** SEM images of **A** $NH_2$-SBA-15 and **B** SH-SBA-15 with different morphologies

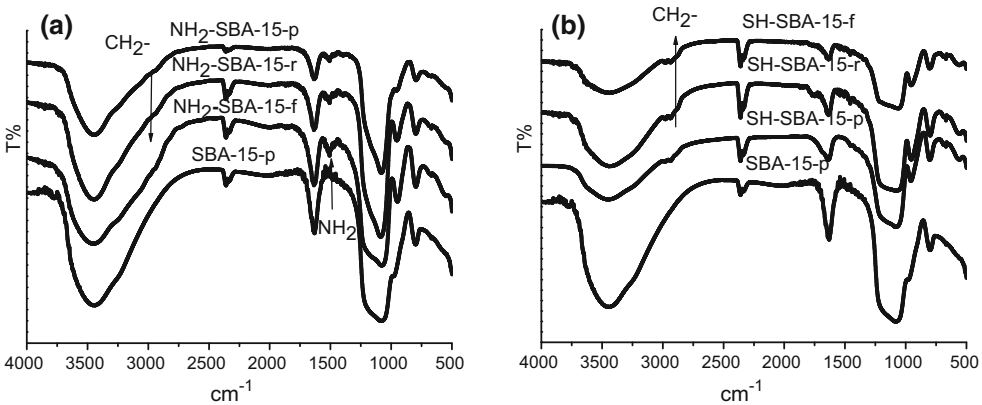


**Fig. 3** FTIR spectra of **a** $NH_2$-SBA-15 and **b** SH-SBA-15 with different morphologies

symmetric $-NH_2$ bending vibration around 1510 $cm^{-1}$ and the weak N–H bending vibration at 690 $cm^{-1}$ confirm the incorporation of amino groups. Even though the signal of the S–H stretching peak (ca. 2580 $cm^{-1}$) in the SH-SBA-15 is too weak to be observed, the $CH_2$ peaks of propyl group at 3000–2750 $cm^{-1}$ indicate that the organic moiety is incorporated. From these results, it can be concluded that organic moieties are indeed bound to the SBA-15 silica.

## Adsorption studies

### *Copper ion adsorption isotherms*

Figure 4a shows the adsorption isotherms of the various adsorbents in removing $Cu^{2+}$ from pH ~ 6 aqueous solutions with different concentrations at 30 °C. Siliceous SBA-15 platelet has a poor affinity for the $Cu^{2+}$ adsorption, while the fibrous $NH_2$-SBA-15 adsorbs 0.3 mmol/g of $Cu^{2+}$, which is a little higher than those of platelet (0.27 mmol/g) and rod-like (0.23 mmol/g). All the isotherms show a large initial slope, indicating that these materials act as high-efficient adsorbents at a low metal concentration of 60 ppm.

Two of the most commonly applied isotherm models: Langmuir and Freundlich, have been adopted to analyze the data. The linear Langmuir and Freundlich expressions are represented as Eqs. (2) and (3).

$$\frac{C_e}{Q_e} = \frac{1}{Q_{max} K_L} + \frac{C_e}{Q_{max}} \tag{2}$$

$$\ln(Q_e) = \ln(K_F) + 1/n \ln(C_e) \tag{3}$$

The fitted isotherms are shown in Fig. 4b, c. The correlation coefficient of Langmuir isotherm ($R^2$ = 0.983–0.999) is higher than that of the Freundlich isotherm ($R^2$ = 0.826–0.983) for the adsorption of copper ion. Hence, only the Langmuir isotherm constants are listed in Table 2. The Langmuir adsorption model is based on the assumption that the monolayer coverage of adsorbate occurs over all equivalent sites, and there are no interactions between adsorbed species. The maximum adsorption capacities $Q_{exp}$ obtained from experiments are in agreement with the $Q_{max}$ values predicted based on Langmuir model. The maximum adsorption capacity decreases in the order of fiber- > platelet- > rod-$NH_2$-SBA-15, and that seems to be proportional to the contents of amino groups on the SBA-15. The fibrous material has the highest loading of amino groups, while the rod-like material contains the least amount of amino groups. Each propylamino group on $NH_2$-SBA-15 is monodentate and provides only one amino position for coordination. The molar ratio (4.1–4.9) of nitrogen to maximum copper adsorbed for $NH_2$-SBA-15 shown in Table 2 suggests that one adsorbed copper ion requires four propylamino groups

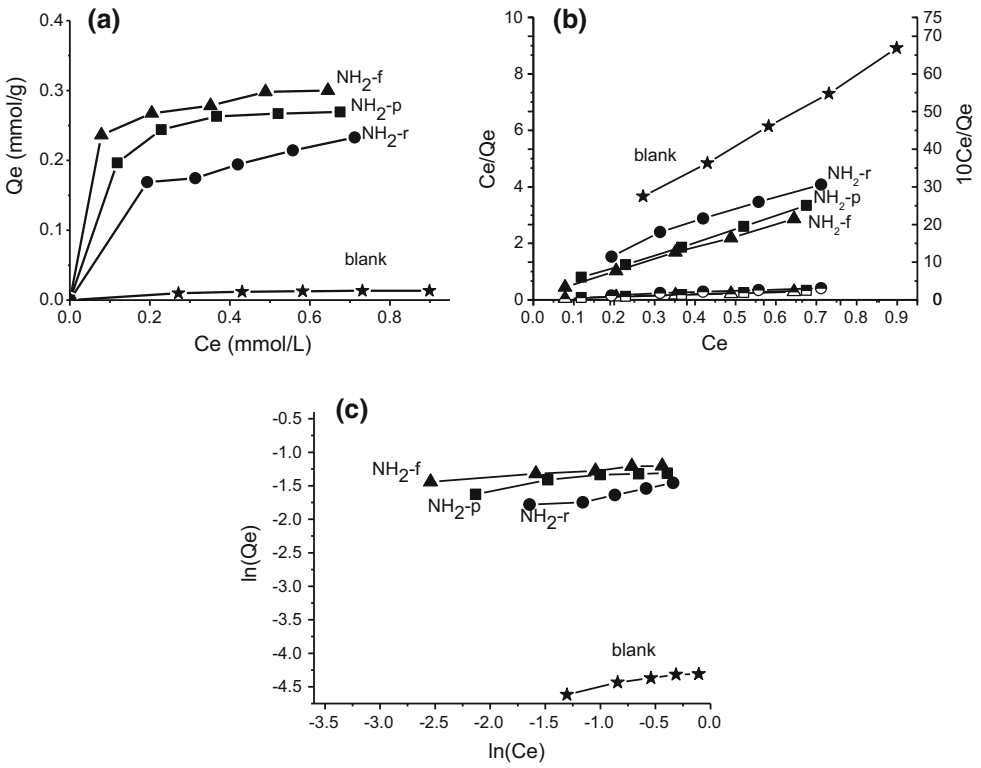


**Fig. 4** Copper ion **a** adsorption isotherms, **b** Langmuir curves (solid: 10Ce/Qe, semisolid: Ce/Qe) and **c** Freundlich curves of $Cu^{2+}$ on various adsorbents at 30 °C, pH ~ 6 aqueous solution with different concentrations of 20, 30, 40, 50, and 60 ppm ($g/m^3$)

**Table 2** Nitrogen contents and maximum $Cu^{2+}$ adsorption, $Q_{exp}$, and Langmuir isotherm constants

| Adsorbents | $N^a$ (mmol/g) | $Q_{exp}$ (mmol/g) | $N/Cu^b$ molar ratio | Langmuir equation | |
|---|---|---|---|---|---|
| | | | | $Q_{max}$ (mmol/g) | $R^2$ |
| Blank (SBA-15-p) | – | 0.013 | – | 0.016 | 0.998 |
| $NH_2$-SBA-15-f | 1.232 | 0.30 | 4.1 | 0.31 | 0.999 |
| $NH_2$-SBA-15-p | 1.228 | 0.27 | 4.6 | 0.29 | 0.999 |
| $NH_2$-SBA-15-r | 1.129 | 0.23 | 4.9 | 0.28 | 0.983 |

[a] From elemental analysis

[b] $N/Q_{exp}$ molar ratio of nitrogen to maximum copper adsorbed. (How many amino groups require per one adsorbed copper ion to form a stable Cu(II)–$NH_2$ complex)

to form a stable Cu(II)–$NH_2$ complex, which is consistent with the literature report (Aguado et al. 2009).

*Time-dependent adsorption capacity*

Figure 5A, B shows the variation in $Pb^{2+}$ and $Cu^{2+}$ uptakes, respectively, on SH-SBA-15 materials with different morphologies in a period of 3 h at 30 °C with initial $Cu^{2+}$ and $Pb^{2+}$ concentrations of 60 ppm (0.94 and 0.29 mmol/L, respectively). The experimental results show rapid initial adsorption rates, followed by a slower rate. The rapid initial adsorption rates are attributed to the large amounts of functional groups available on the absorbents to bind with the metal ions (Lam et al. 2006). Furthermore, the metal ion concentration in the aqueous solution is higher initially, and this results in a higher adsorption rate. After the initial period, slow adsorption may be due to the less amounts of functional groups available on the absorbents and a lower metal ion concentration remaining in the aqueous solution. It is noticed that a significant leaching of the $Cu^{2+}$ ions from SH-SBA-15 adsorbents of all morphologies to aqueous solutions was observed after 2–10 min of contact time up to ca. 60 min (Fig. 5Ba). Similarly, leaching of $Cu^{2+}$ ions is seen from platelet $NH_2$-SBA-15 (Fig. 6Ba) and to a much less extent for $Pb^{2+}$ from $NH_2$-SBA-15 (Fig. 6Aa). This phenomenon implies that

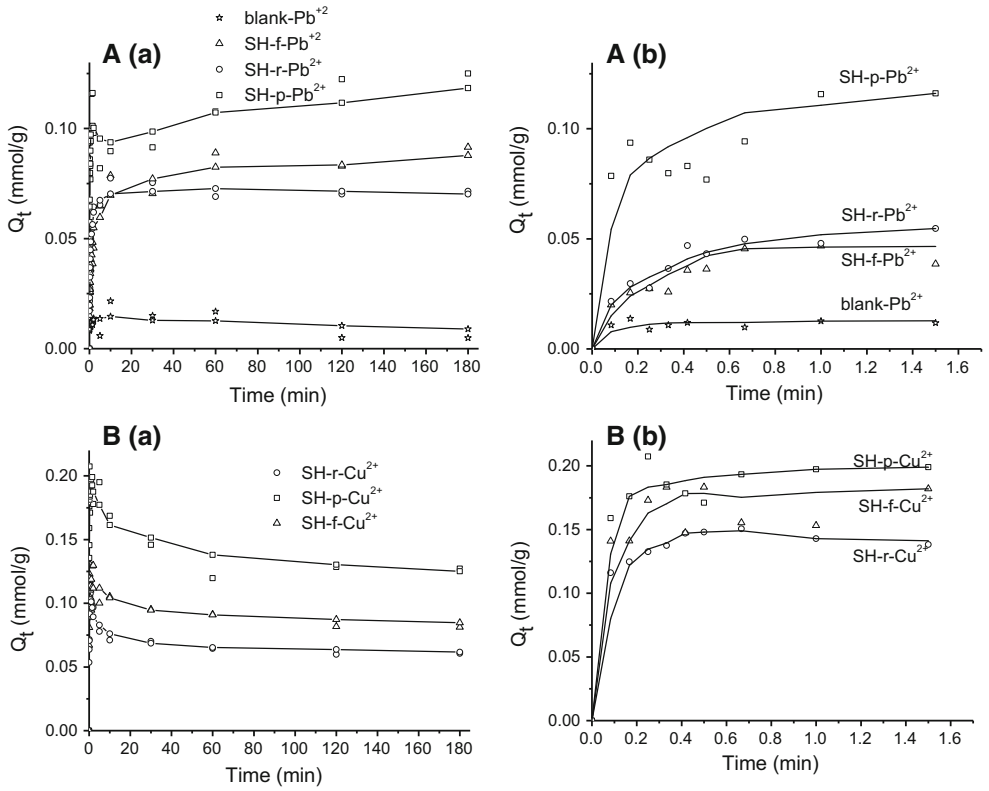


**Fig. 5** Kinetics curves for absorption of $Pb^{2+}$ (**A**) and $Cu^{2+}$ (**B**) ions in pH ~ 6 aqueous solutions on SH-SBA-15 materials with different morphologies, at 30 °C and initial $Cu^{2+}$ and $Pb^{2+}$ concentrations 60 ppm (mg/L) for **a** long period (3 h) and **b** short period (1.5 min)

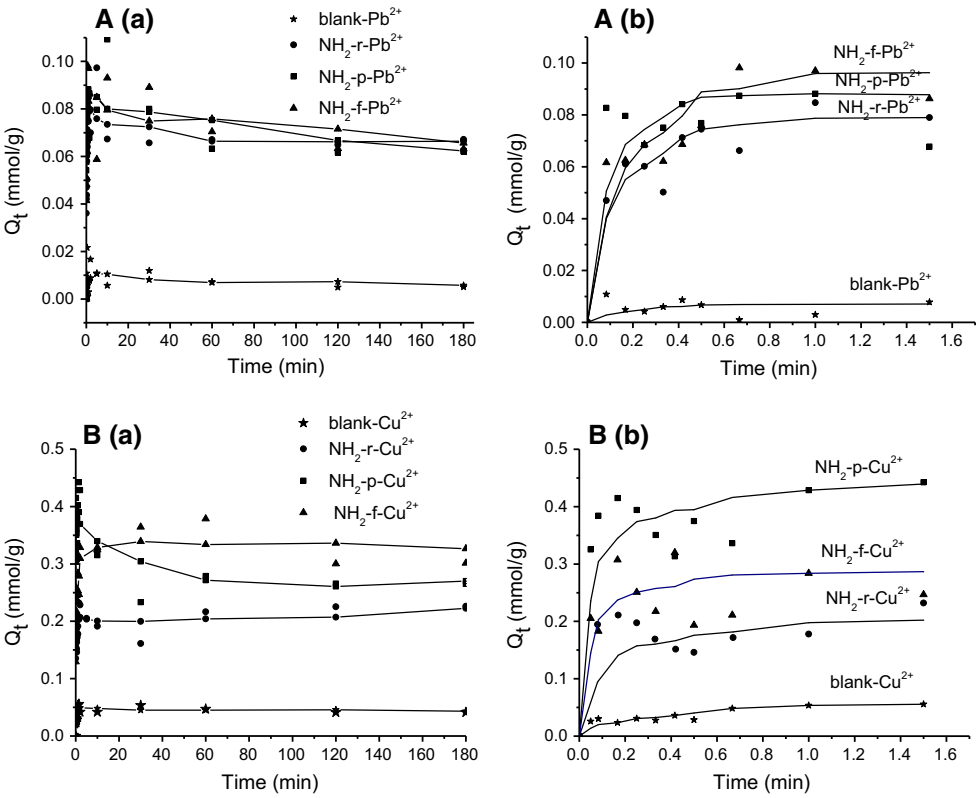


**Fig. 6** Kinetics curves for absorption of $Pb^{2+}$ (**A**) and $Cu^{2+}$ (**B**) ions in pH ~ 6 aqueous solutions on $NH_2$-SBA-15 materials with different morphologies at 30 °C and initial $Cu^{2+}$ and $Pb^{2+}$ concentrations 60 ppm (mg/L) for **a** long period (3 h) and **b** short period (1.0 min)

the complexes formed in the early stage of absorption are probably not stable. Although M-L coordinating bonds are formed, the number of ligand per metal is lower than that of stable complexes. As the absorption proceeds, the metals absorbed rearrange the coordinating environment around the functional groups. The extra metal ions are released into the solution "as the equilibrium complexes take away their ligands."

In the long-term adsorption diagram (Fig. 5Aa), platelet SH-SBA-15 adsorbs 0.125 mmol/g of $Pb^{2+}$, rod-like 0.072 mmol/g, and fiber-like 0.092 mmol/g. On the other hand, Fig. 5Ba shows that the $Cu^{2+}$ uptakes for the same three adsorbents are 0.127, 0.061, and 0.081 mmol/g, respectively. Although the adsorption capacities of $Pb^{2+}$ and $Cu^{2+}$ are similar to each other for SH-SBA-15 of the same morphology, it should be noted that the initial molar concentrations of $Cu^{2+}$ is much higher than that of $Pb^{2+}$. If the effect of initial molar concentrations is considered, all the SH-SBA-15 absorbents will have higher uptakes of $Pb^{2+}$ ions than $Cu^{2+}$ ions.

The uptakes of metal ions per site on functionalized SBA-15 with varied morphologies and the distribution coefficient ($K_d$) are summarized in Table 3. For thiol-functionalized SBA-15, the uptakes of $Cu^{2+}$ and $Pb^{2+}$ per site are similar for specific morphology. However, platelet materials always have higher cation uptakes. Significant differences are observed on the $K_d$ values. For $Pb^{2+}$ ions

**Table 3** $Cu^{2+}$ and $Pb^{2+}$ uptake capacities for SH-SBA-15 and $NH_2$-SBA-15 adsorbents

| Adsorbents | Uptake[a] $Cu^{2+}$/site | $K_d$ (L/g)[b] $Cu^{2+}$ | Uptake[a] $Pb^{2+}$/site | $K_d$ (L/g)[b] $Pb^{2+}$ |
|---|---|---|---|---|
| SH-SBA-15-p | 0.118 | 0.155 | 0.120 | 0.76 |
| SH-SBA-15-r | 0.070 | 0.069 | 0.083 | 0.33 |
| SH-SBA-15-f | 0.078 | 0.094 | 0.085 | 0.46 |
| $NH_2$-SBA-15-p | 0.215 | 0.39 | 0.050 | 0.27 |
| $NH_2$-SBA-15-r | 0.20 | 0.31 | 0.059 | 0.30 |
| $NH_2$-SBA-15-f | 0.245 | 0.47 | 0.051 | 0.28 |

In pure water (pH ~ 6), 30 °C, initial concentration of $Cu^{2+}$ and $Pb^{2+}$ was 60 ppm (0.94 and 0.29 mmol/L, respectively)

[a] Q/FG (functional group) contents

[b] $K_d = Q/C_e$ (adsorption efficiency)

absorbed on SH-SBA-15 of different morphologies, the $K_d$ values increase from 0.33 (rod-like), 0.46 (fibrous) to 0.76 (platelet). In comparison, the $K_d$ values for $Cu^{2+}$ ions on the SH-SBA-15 are much smaller: 0.069 (rod-like), 0.094 (fibrous) to 0.155 (platelet). These results indicate that the affinity between thiol groups and $Pb^{2+}$ ions is stronger than that of $Cu^{2+}$ ions.

The morphology effect on the initial adsorption rate can be observed clearly from the short-time adsorption process. The initial adsorption rates for both $Cu^{2+}$ and $Pb^{2+}$ ions onto the platelet SH-SBA-15 adsorbents are rapid and are

faster than those of the fibrous- and the rod-like morphologies. These results prove that the short channeling pores of the platelet morphology facilitate the diffusion of the solvated cations and migration through the channeling pores during the adsorption processes.

For the amino-functionalized SBA-15, Fig. 6Ba shows that platelet adsorbs 0.265 mmol/g, rod-like 0.226 mmol/g, and fiber-like 0.301 mmol/g of $Cu^{2+}$, while only 0.062, 0.067, and 0.063 mmol/g of $Pb^{2+}$ are adsorbed in the same three adsorbents, respectively, as shown in Fig. 6Aa. In other words, $NH_2$-SBA-15 has a much larger adsorption capacities of $Cu^{2+}$ than $Pb^{2+}$. From the initial absorption period shown in Fig. 6Ab, Bb, higher initial adsorption rates of both $Cu^{2+}$ and $Pb^{2+}$ are also observed for the platelet $NH_2$-SBA-15 than those of the other two morphologies.

From the uptakes of metal ions per site and distribution coefficient ($K_d$) summarized in Table 3, thiol-functionalized SBA-15 adsorbents of all morphologies have higher $Pb^{2+}$ adsorbed per site than that of the amino-functionalized SBA-15. The $K_d$ values of $Pb^{2+}$ on SH-SBA-15 of different morphologies are higher than those obtained on $NH_2$-SBA-15; especially, the highest $K_d$ value is obtained on platelet SH-SBA-15. These results demonstrate that the thiol-functionalized mesoporous materials are more efficient adsorbents for $Pb^{2+}$ than $Cu^{2+}$. On the contrary, $NH_2$-SBA-15 materials show much better adsorption capacity per site for $Cu^{2+}$ than that of SH-SBA-15 materials. Under the same pH and initial solute concentration, pore size, the quantity, and nature of the functional group are the main factors affecting the metal adsorptions (Lam et al. 2006; Walcarius et al. 2003; Vasudevan et al. 2011; Blitz et al. 2007; Aguado et al. 2009; Xia et al. 2010). Aguado et al. (2009) studied adsorption of heavy metal ions by SBA-15 materials functionalized with various amino-containing groups prepared by both one-pot condensation and grafting methods. However, they observed no detectable amounts of metal adsorption by the materials prepared by co-condensation. That is completely different from our observations here. Both $NH_2$-SBA-15 and SH-SBA-15 materials prepared by co-precipitation showed good absorption capacities toward $Cu^{2+}$ (up to 0.3 mmol/g or 19 mg/g) and $Pb^{2+}$ ions (up to 0.067 mmol/g, or 13.8 mg/g). Possible reason was that the materials reported (Aguado et al. 2009) were not pretreated with base solution to neutralize the ammonium groups formed in the acid-synthesis condition of SBA-15. As a result, the amino-functional groups could not coordinate with metal ions.

Here, morphology is shown to be an important factor affecting the metal ions adsorption. The absorbed $Pb^{2+}$ per site of SH-SBA-15 with platelet morphology, which has the largest pore diameter (Table 1) among the six adsorbents, is much higher than those of the other five materials in Table 3. The channel length of the platelet materials is shorter than those of fibrous and rod-like materials, and it decreases the diffusion distance and time for metal ions to migrate from the bulk solution into the interior of the adsorbents where the majority of functional groups were incorporated. Also, the larger pore size may have less hindrance for the absorbed species to block the diffusion of metal ions inside the interior of channels (Liu et al. 2000).

In Table 3, the $Cu^{2+}$ uptake per site and the $K_d$ of $Cu^{2+}$ on amino-functionalized SBA-15 materials are larger than those obtained for SH-SBA-15. In contrast, the $Pb^{2+}$ uptake per site and the $K_d$ of $Pb^{2+}$ on thiol-functionalized SBA-15 materials are larger than those obtained on $NH_2$-SBA-15. These results may be explained by the hard and soft acids and bases (HSAB) theory. According to HSAB theory of Pearson (1963), $Cu^{2+}$ and $Pb^{2+}$ are the borderline metals with ambivalent properties that show that the absolute hardness of amino and thiol group is 5.3 and 4.1, respectively, while that of $Cu^{2+}$ and $Pb^{2+}$ is 8.5 and 8.3, respectively (Parr and Pearson; 1983). Soft metal ions tend to form stable complexation with ligands containing soft donor atoms. Nitrogen is regarded as a harder donor atom than sulfur. Therefore, the amino-functionalized adsorbents exhibit a higher complexing affinity for the harder metal ion $Cu^{2+}$, while thiol-functionalized adsorbents show a greater complexation affinity for the softer metal ion $Pb^{2+}$.

## Effect of pH

The effects of initial pH values of $Pb(NO_3)_2$ and $Cu(NO_3)_2$ solutions on the adsorption onto SH-SBA-15-p and $NH_2$-SBA-15-p at pHs of 2–6 are illustrated in Fig. 7b. The adsorption of $Pb^{2+}$ on SBA-15-p (blank) was negligible. The uptake of $Pb^{2+}$ on SH-SBA-15-p increases with solution pH values. The SH-SBA-15-p has an isoelectric point (from Fig. 7a) at around the pH of 2.8, and SH groups are protonated at a pH lower than this value. The reason may be that at lower pH, the protonation of the S atom of the –SH group diminishes its ability in complex formation with lead ions. The uptake of $Cu^{2+}$ on $NH_2$-SBA-15-p also increases with solution pH from 2 to 5. The isoelectric point of $NH_2$-SBA-15-p is estimated to be 7.3, and below this pH, the surface of adsorbents is positively changed. The maximal adsorption of $Cu^{2+}$ ions onto $NH_2$-SBA-15 is at pH 5. It is because protonated amino groups ($NH_3^+$) are deprotonated with the increase in pH and more amino groups are available for coordination with $Cu^{2+}$ ions (Lam

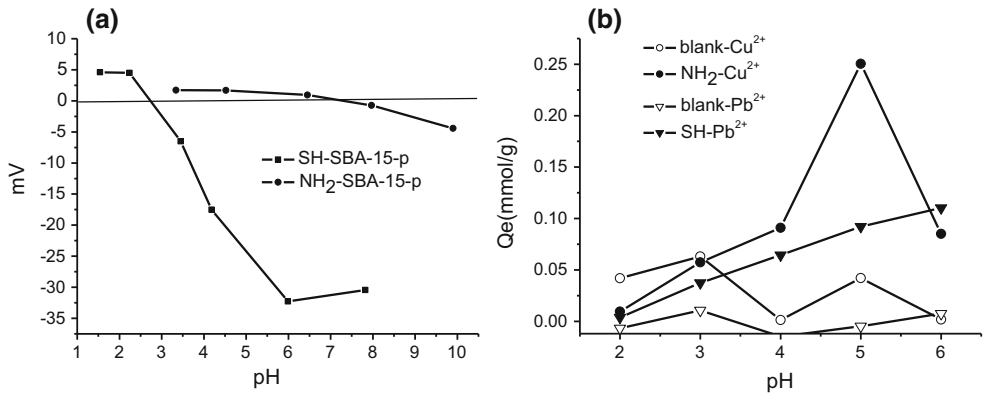


**Fig. 7** **a** Zeta potential of SH-SBA-15-p and $NH_2$-SBA-15-p adsorbents as a function of solution pH, **b** effect of pH on the adsorption capacities of $Cu^{2+}$ and $Pb^{2+}$ onto $NH_2$-SBA-15-p and SH-SBA-15-p at 30 °C, $C_o = 60$ ppm

et al. 2006; Da'na and Sayari 2011; Shahbazi et al. 2011). Also, at very low pH, the concentration of hydrogen ions is high, directly competing with $Cu^{2+}$ for active binding sites (Shahbazi et al. 2011). Above pH 5, the adsorption decreases and due to that, $Cu^{2+}$ will form precipitate $Cu(OH)_2$ near pH 6 ($K_{sp} = 1.6 \times 10^{-19}$), and hence, adsorption capacity drops. This is a similar trend as that for tea waste adsorbing copper ions (Amarasinghe and Williams 2007).

## Conclusion

A series of amino- and thiol-functionalized SBA-15 materials were synthesized to study the adsorption behavior of $Cu^{2+}$ and $Pb^{2+}$ in solution at 30 °C. With the aid of proper amount of Zr(IV) and NaCl salt, amino- and thiol-functionalized SBA-15 materials with different morphologies and different lengths of channeling pores were prepared.

The equilibrium data of copper adsorption fitted well to Langmuir isotherms. Moreover, they revealed that four amino groups are required to form a stable surface complex with $Cu^{2+}$. The experimental results of kinetics showed rapid initial adsorption rate followed by a slower rate. Adsorption kinetics indicated that the initial adsorption rate onto platelet mesoporous adsorbents is rapid and faster than the rates of rod-like and fiber-like morphologies. This advantage is applicable to chemical catalysis where the reaction rate may be enhanced and in sensor devices where the response time can be reduced.

The thiol-group SBA-15 adsorbents of all the morphologies have a better affinity for $Pb^{2+}$ than the amino-group SBA-15 does. In contrast, the amino-group SBA-15 has a stronger affinity for $Cu^{2+}$ compared to thiol-group SBA-15. The HSAB theory was used to explain these phenomena. The uptake of $Pb^{2+}$ per site on SH-SBA-15 with platelet morphology is much higher than that of the other materials although its pore size is also the largest among the materials. Hence, the morphology is an important factor affecting the metal ions adsorption in the experimental conditions under observation. The $Pb^{2+}$ uptake onto thiol-SBA-15-p increases between pH of 2 and 6. The adsorption capacity for $Cu^{2+}$ onto the amino-SBA-15-p increases between pH of 2 and 5, and it drops at pH of 6. This phenomenon can be explained by the protonation of the thiol- and amino-functional groups at low-pH condition, and the adsorbents lose the complexing capabilities with $Cu^{2+}$ and $Pb^{2+}$.

**Acknowledgments** The financial supports from the Ministry of Science and Technology (NSC 101-2113-M-002-012-MY3) and Ministry of Education, Taiwan, are gratefully acknowledged. Acknowledgements are also extended to C. W. Lu for CHNS elemental analysis, and C. Y. Lin and S. J. Ji for EM measurement at Instrumentation Center, National Taiwan University.

## References

Agnado J, Arsuaga JM, Arencibia A (2008) Influence of synthesis conditions on mercury adsorption capacity of propylthiol

functionalized SBA-15 obtained by co-condensation. Microporous Mesoporous Mater 109:513–524
Aguado J, Arsuaga JM, Arencibia A, Lindo M, Gascon V (2009) Aqueous heavy metals removal by adsorption on amine-functionalized mesoporous silica. J Hazard Mater 163:213–221
Amarasinghe BMWPK, Williams RA (2007) Tea waste as a low cost adsorbent for the removal of Cu and Pb from wastewater. Chem Eng J 132:299–309
Beck JS, Vartuli JC, Roth J, Lenowicz ME, Kresge CT, Schmidt KD, Chu CTW, Olson DH, Sheppard EW, McCullen SB, Higgins JB, Schlenker JL (1992) A new family of mesoporous molecular sieves prepared with liquid crystal templates. J Am Chem Soc 114:10834–10843
Blitz IP, Blitz JP, Gun'ko VM, Sheeran DJ (2007) Functionalized silicas: structural characteristics and adsorption of Cu(II) and Pb(II). Colloids Surf A Physicochem Eng Asp 307:83–92
Chandra D, Das SK, Bhaumik A (2010) Afluorophore grafted 2D-hexagonal mesoporous organosilica: excellent ion-exchanger for the removal of heavy metal ions from wastewater. Microporous Mesoporous Mater 128:34–40
Chen S, Huang CY, Yokoi T, Tang CY, Huang SJ, Lee JJ, Tsai YL, Chan CY, Liu YC, Chang S (2008) A facile route to synthesizing functionalized mesoporous SBA-15 materials with platelet morphology and short mesochannels. Chem Mater 20:3906–3916
Chen SY, Huang CY, Yokoi T, Tang CY, Huang SJ, Lee JJ, Chan JCC, Tatsumi T, Cheng S (2012) Synthesis and catalytic activity of amino-functionalized SBA-15 materials with controllable channel lengths and amino loadings. J Mater Chem 22:2233–2243
Da'na E, Sayari A (2011) Adsorption of copper on amine-functionalized SBA-15 prepared by co-condensation: equilibrium properties. Chem Eng J 166:445–453
Deng S, Bai R, Chen JP (2003) Aminated polyacrylonitrile fibers for lead and copper removal. Langmuir 19:5058–5064
Dufaud V, Davis ME (2003) Design of heterogeneous catalysts via multiple active site positioning in organic–inorganic hybrid materials. J Am Chem Soc 125:9403–9413
Feng X, Fryxell GE, Wang LQ, Kim AY, Liu J, Kemner KM (1997) Functionalized monolayers on ordered mesoporous supports. Science 276:923–926
Kao HM, Shen TY, Wu JD, Lee LP (2008) Control of ordered structure and morphology of cubic mesoporous silica SBA-1 via direct synthesis of thiol-functionalization. Microporous Mesoporous Mater 110:461–471
Kosuge K, Sato T, Kikukawa N, Takemori M (2004) Morphological control of rod- and fiberlike SBA-15 type mesoporous silica using water-soluble sodium silicate. Chem Mater 16:899–905
Lacour S, Bollinger JC, Serpaud B, Chantron P, Arcos R (2001) Removal of heavy metals in industrial wastewaters by ion-exchanger grafted textiles. Anal Chim Acta 428:121–132
Lam KF, Yeung KL, McKay G (2006) Rational approach in the design of selective mesoporous adsorbents. Langmuir 22:9632–9641
Liang X, Xu Y, Sun G, Wang L, Sun Y, Qin X (2009) Preparation, characterization of thiol-functionalized silica and application for sorption of $Pb^{2+}$ and $Cd^{2+}$. Collids Surf A Physicochem Eng Asp 349:61–68
Linton P, Alfredsson V (2008) Growth and morphology of mesoporous SBA-15 particles. Chem Mater 20:2878–2880
Liu AM, Hidajat S, Zhao DY (2000) A new class of hybrid mesoporous materials with functionalized organic monolayers for selective adsorption of heavy metal ions. Chem Commun 13:1145–1146
Melero JA, Grieken RV, Morales G (2006) Advances in the synthesis and catalytic applications of organosulfonic-functionalized mesostructured materials. Chem Rev 106:3790–3814
Özcan AS, Gok O, Özcan A (2009) Adsorpption of lead(II) ions onto 8- hydroxyl quinoline- immobilized bentonite A. J Hazard Mater 161:499–509
Parr RG, Pearson RG (1983) Absolute hardness: companion parameter to absolute electronegativity. J Am Chem Soc 105:7512–7516
Pearson RG (1963) Hard and soft acids and bases. J Am Chem Soc 85:3533–3539
Sayari A, Han BH, Yang Y (2004) Simple synthesis route to monodispersed SBA-15 silica rods. J Am Chem Soc 126:14348–14349
Shahbazi A, Younesi H, Badiei A (2011) Functionalized SBA-15 mesoporous silica by melamine-based dendrimer amines for adsorptive characteristics of Pb(II), Cu(II) and Cd(II) heavy metal ions in batch and fixed bed column. Chem Eng J 168:505–518
Sharaf G, Hassan H (2014) Removal of copper ions from aqueous solution using silica derived from rice straw: comparison with activated charcoal. Int J Environ Sci Technol 11:1581–1590
Singh J, Ali A, Prakash V (2014) Removal of lead(II) from synthetic and batteries wastewater using agricultural residues in batch/-column mode. Int J Environ Sci Technol 11:1759–1770
Sujandi Prasetyato EA, Park SE (2008) Synthesis of short-channeled amino-functionalized SBA-15 and its beneficial applications in base-catalyzed reactions. Appl Catal A 350:244–251
Vasudevan M, Sakaria PL, Bhatt AS, Mody HM, Bajaj HC (2011) Effect of concentration of aminopropyl groups on the surface of MCM-41 on adsorption of $Cu^{2+}$. Ind Eng Chem Res 50:11432–11439
Walcarius A, Etienne M, Lebean B (2003) Rate of access to the binding sites in organically modified silicates. 2. Ordered mesoporous silicas grafted with amine or thiol groups. Chem Mater 15:2161–2173
Wang LH, Lin CI (2008) Adsorption of lead(II) ion from aqueous solution using rice hull ash. Ind Eng Chem Res 47:4891–4897
Wang X, Lin KSK, Chan JCC, Cheng S (2005) Direct synthesis and catalytic applications of ordered large pore aminopropyl-functionalized SBA-15 mesoporous materials. J Phys Chem B 109:1763–1769
World Health Organization (2006) Guidelines for drinking-water quality, 3rd edn. World Health Organization, Geneva, p 54
Xia K, Ferguson RZ, Losier M, Tchoukanova N, Bruning R, Djaoued Y (2010) Synthesis of hybrid silica materials with tunable pore structures and morphology and their application for heavy metal removal from drinking water. J Hazard Mater 183:554–564
Yu C, Fan J, Tian B, Zhao D, Stucky GD (2002) High-yield synthesis of periodic mesoporous silica rod and their replication to mesoporous carbon rods. Adv Mater 14:1742–1745
Yu C, Fan J, Tian B, Zhao D (2004) Morphology development of mesoporous materials: a colloidal phase separation mechanism. Chem Mater 16:889–898
Zhang H, Sun J, Ma D, Weinberg G, Su DS, Bao X (2006) Engineered complex emulsion system: toward modulating the

pore length and morphological architecture of mesoporous silicas. J Phys Chem B 110:25908–25915

Zhao D, Huo Q, Feng J, Chmelka BF, Stucky GD (1998a) Nonionic triblock and star diblock copolymer and oligomeric surfactant syntheses of highly ordered, hydrothermally stable, mesoporous silica structures. J Am Chem Soc 120:6024–6036

Zhao D, Feng J, Huo Q, Melosh N, Frederickson GH, Chmelka BF, Stucky GD (1998b) Triblock copolymer syntheses of mesoporous silica with periodic 50 to 300 Angstrom pores. Science 279:548–552

Zhao D, Sun J, Li Q, Stucky GD (2000) Morphological control of highly ordered mesoporous silica SBA-15. Chem Mater 12:275–279